Vibronic Structure and Coupling in the Electronic Spectra of the Hexacarbonyl Tantalate(I−) Ion

Theodore W. Bitner and Jeffrey I. Zink*

Contribution from the Department of Chemistry and Biochemistry, University of California, Los Angeles, California 90095

Received March 23, 2000

Abstract: Emission, excitation, and vibrational spectra of $[Ph_4P][Ta(CO)_6]$ are reported. The emission spectrum is assigned to a ligand field transition and contains a well-resolved vibrational progression in the symmetric Ta−C stretching normal mode. A second progression at longer wavelength is separated from the first by an energy that superficially does not appear to correspond to a vibrational mode. The spectra are interpreted in terms of Herzberg−Teller (H−T) coupling of the forbidden ligand field state with the fully allowed tantalum-to-carbonyl charge-transfer excited-state mediated by asymmetric t_{1u} normal modes. The H−T coupling is treated by using a coordinate-dependent transition dipole moment that is zero at the equilibrium internuclear geometry but becomes nonzero along appropriate asymmetric normal coordinates. The coordinate dependence of the transition dipole moment is illustrated by using simple overlap considerations. Quantitative calculations of the spectra are carried out using the time-dependent theory of electronic spectroscopy and the coordinate-dependent transition dipole. The emission spectrum originates from a single excited electronic state with a single origin but two H−T false origins. Changes of the Ta−C and C−O bond lengths in the emitting excited electronic state are calculated and discussed. Alternative interpretations of the spectrum based on two emitting molecules, sites, or excited states are eliminated by excitation spectroscopy and by temperature, lifetime, and solvent dependence studies of the emission.

Introduction

Vibronic structure in electronic spectra can provide important information about bond length and angle changes in excited electronic states.[1−3] However, in large metal-containing molecules the structure is often obscured because overlapping electronic bands and the large number of displaced normal modes result in congested spectra. Luminescence spectroscopy can be a useful tool for obtaining detailed information about the lowest energy excited electronic state. Optical emission spectra usually consists of one band corresponding to a transition from only the lowest energy excited state, and the problems caused by overlapping bands from transitions to multiple states nearby in energy are eliminated. Radiationless deactivation often prevents luminescence spectroscopy from being used.

As part of our interest in excited-state distortions of organometallic compounds, we have been examining the luminescence spectra of metal carbonyls.[4−6] These spectra often contain unusual vibronic features that lead to new insight into vibronic interactions. For example, the emission spectra of $W(CO)_5$(pyridine) and $W(CO)_5$(piperidine) contained the first examples of the missing mode effect (MIME).[4] Homoleptic metal carbonyl compounds are prototypical textbook examples for illustrating the electronic structure of organometallic compounds, but luminescence from these types of compounds (with the exception of d,[6] 18-electron group V compounds)[7] is very rare, and the vibronic properties are relatively unknown.[8,9]

The low-temperature emission spectrum of the tantalum hexacarbonyl anion, $[Ta(CO)_6]^-$, contains unexpected vibronic structure. The structure, shown in Figure 1, appears at first glance to be composed four regularly spaced peaks, a gap, and a second set of regularly spaced peaks. The peaks on the high-energy side of the gap are labeled the "blue" peaks, and the set of peaks to lower energy are labeled the "red" peaks. A simple interpretation is that both sets of peaks originate from one electronic state with vibrational progressions in a low-frequency (metal−ligand) mode separated by a high-frequency (carbonyl stretching) vibration. An alternative explanation is that the sets of peaks are due to dual emissions arising from two different electronic states, emission from molecules in two crystal defect sites, or emission from an impurity similar to the molecule. We systematically eliminate these possibilities and show that the red and blue progressions are the result of vibronic coupling between electronic states.

In this paper we analyze the vibronic structure in the emission spectrum in terms of Herzberg−Teller coupling between the lowest energy ligand field state and the nearby metal−ligand

(1) Herzberg, G. *Electronic Spectra of Polyatomic Molecules III: Electronic Spectra and Electonic Structure of Polyatomic Molecules*; Van Nostrand Reinhold: Cincinnati, OH, 1966.

(2) *Electronic and Vibronic Spectra of Transition Metal Complexes I*; Yersin, H., Ed.; Springer-Verlag: New York, 1994.

(3) Zink, J. I.; Kim-Shin, K. S. Molecular distortions in excited electronic states determined from electronic and resonance Raman spectroscopy. In *Advances in Photochemistry*, Vol. 16; Volman, D. H., Hammond, G. S., Neckers, D. C., Eds.; John Wiley and Sons: New York, 1991; p 119.

(4) (a) Tutt, L.; Tannor, D.; Heller, E. J.; Zink, J. I. *Inorg. Chem.* **1982**, *21*, 3859. (b) Tutt, L.; Tannor, D.; Schindler, J.; Heller, E. J.; Zink, J. I. *J. Phys. Chem.* **1983**, *87*, 3017. (c) Tutt, L.; Zink, J. I.; Heller, E. J. *Inorg. Chem.* **1987**, *26*, 2158.

(5) Tutt, L.; Zink, J. I. *J. Am. Chem. Soc.* **1986**, *108*, 5830.

(6) Larson, L. J.; Oskam, A.; Zink, J. I. *Inorg. Chem.* **1991**, *30*, 42.

(7) Wrighton, M. S.; Handell, D. I.; Morse, D. I. *Inorg. Chem.* **1976**, *15*, 434.

(8) McHugh, T. M.; Narayanaswamy, R.; Rest, A. J.; Salisbury, K. *J. Chem. Soc., Chem. Commun.* **1979**, 208.

(9) Lees, A. *Chem. Rev.* **1987**, *87*, 711.

10.1021/ja0010305 CCC: $19.00
Published on Web 10/13/2000

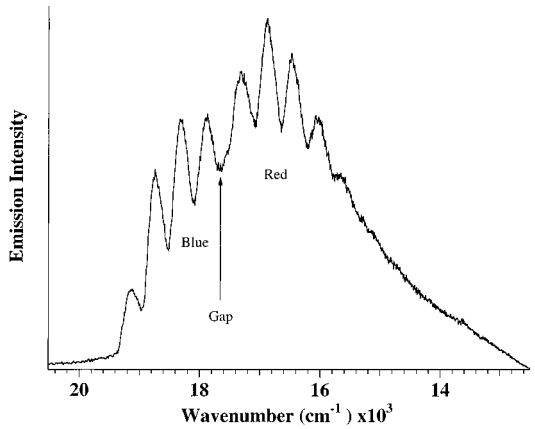

Figure 1. Experimental emission spectrum of $[Ta(CO)_6]^-$ taken at 15 K. Two sets of equally spaced progressions, labeled red and blue, are separated by a gap.

charge transfer state. The emission spectrum results from two symmetric normal modes (the Ta−C and the C−O stretching modes) built on two t_{1u} promoting modes producing two false origins. One of the vibronic origins involves a low-frequency asymmetric metal−ligand normal mode, while the second involves the high-frequency asymmetric carbonyl stretching vibration. We quantitatively calculate the emission spectrum by using the time-dependent theory of electronic spectroscopy. The two false origins are calculated by using a coordinate-dependent transition dipole moment that changes sign at the origin. We derive the coordinate dependence from a simple graphical overlap picture that illustrates why the transition is forbidden at the internuclear ground-state equilibrium geometry but becomes allowed by asymmetric vibrations. Finally, we calculate the bond length changes in the excited ligand field electronic state and compare these changes to those in other metal carbonyl compounds.

Experimental Section

The title compound $[Ph_4P][Ta(CO)_6]$ was synthesized by using literature methods.[10,11] Elemental analysis shows that the compound is analytically pure. The compound is air sensitive, and all spectra were obtained from samples in sealed capillaries that were assembled in a drybox.

Emission Spectra. Luminescence spectra taken at 15 K were obtained using a Spex 1702 single monochromator equipped with a Hamamatsu R316-02 red-sensitive photomultiplier tube. The signal was recorded with a Stanford Research System SR400 photon counter and a personal computer. The 363.8-nm line from a Coherent I-90 argon ion laser at 5 mW was used for excitation. Microcrystalline solid samples were cooled inside an Air Products closed-cycle helium refrigerator displex equipped with a thermocouple. The spectra are corrected for the instrument's response.

Emission spectra were also obtained at 77 K by using an ISA Spex model FL-22 Fluorolog. These spectra were taken in conjunction with the excitation experiments.

Excitation Spectra. Excitation spectra taken at 15 K were obtained using the monochromator described above. The sample was excited by the visible output of an Opotech Optical Parametric Oscillator pumped by the 355-nm output of a tripled Nd:YAG laser. The spectra were scanned from high to low energy over the wavelength range of 410−560 nm. The pulse energy used for sample irradiation was approximately 0.05−0.1 mJ/pulse. Data were collected using an SRS gated integrator and boxcar averager. Samples were cooled inside an Air Products closed-cycle helium refrigerator displex equipped with a thermocouple. Intensity fluctuations of the laser output were corrected by monitoring the luminescence intensity of a solution of Rhodamine 640 placed in front of a 1P28 reference photomultiplier tube.

Continuous-wave excitation spectra were taken at 77 K by using an ISA Spex model FL3-22 Fluorolog. The excitation spectra were corrected for the intensity of the xenon lamp irradiation source.

Raman Spectra. Spectra were obtained at room temperature using a Spex 1401 double monochromator equipped with an RCA C31034 photomultiplier tube. Data were collected with a Stanford Research System SR400 photon counter and stored on an IBM PC computer. The 676.4-nm line from a Coherent I-90K krypton laser at 25 mW was used for excitation. All vibrational spectra were calibrated against solid Bi_2O_3 and have uncertainties of ± 2 cm^{-1}.

Emission Spectra in a Frozen Organic Glass. Spectra were obtained using a Spex 1401 double monochromator equipped with an RCA C31034 photomultiplier tube. Data were collected with a Stanford Research System SR400 photon counter and stored on an computer. The 363.8-nm line from a Coherent I-90 argon laser was used for excitation. The title compound was diluted in purified and degassed methyl-tetrahydrofuran. Samples were cooled to 15 K using the closed-cycle liquid helium displex described above.

Emission Lifetime Measurements. Lifetime measurements were obtained by exciting the sample using the 10-ns, 406-nm output of a Spectra-Physik XeCl excimer-pumped dye laser at 40 Hz. The emission decay was monitored at 18 768 and 16 515 cm^{-1} using the Spex single monochromator described above with the slits set at 250 μm.

Table 1. Vibronic Peak Maxima in the $[Ta(CO)_6]^-$ 15 K Emission Spectrum

energy (cm^{-1})	$\omega^{n+1} - \omega^n$	assignment
19 530		forbidden electronic origin
19 130		$\hbar\omega(t_{1u}^{400}) + 0\hbar\omega(a_{1g}^{410})$
18 737	393	$\hbar\omega(t_{1u}^{400}) + 1\hbar\omega(a_{1g}^{410})$
18 325	412	$\hbar\omega(t_{1u}^{400}) + 2\hbar\omega(a_{1g}^{410})$
17 892	432	$\hbar\omega(t_{1u}^{400}) + 3\hbar\omega(a_{1g}^{410})$
(17 685)	obscured[a]	$\hbar\omega(t_{1u}^{1845}) + 0\hbar\omega(a_{1g}^{410})$
17 500 (sh)	392[a]	$\hbar\omega(t_{1u}^{400}) + 4\hbar\omega(a_{1g}^{410})$
17 352	(ref)[b]	$\hbar\omega(t_{1u}^{1845}) + 1\hbar\omega(a_{1g}^{410})$
16 878	474	$\hbar\omega(t_{1u}^{1845}) + 2\hbar\omega(a_{1g}^{410})$
16 477	401	$\hbar\omega(t_{1u}^{1845}) + 3\hbar\omega(a_{1g}^{410})$
16 072	405	$\hbar\omega(t_{1u}^{1845}) + 4\hbar\omega(a_{1g}^{410})$
15 657	415	$\hbar\omega(t_{1u}^{1845}) + 5\hbar\omega(a_{1g}^{410})$

[a] These weak peaks are at wavenumbers that lie within the 540-cm^{-1} gap between the 17 892- and 17 352-cm^{-1} peaks. [b] This peak is 410 cm^{-1} away from the expected position of the obscured peak at 17 685 cm^{-1}. [c] The average vibronic spacing for all of the observed peaks is 410 cm^{-1}, with a standard deviation of $\pm$ 10 cm^{-1}. The 540-cm^{-1} energy separation between the 17 892- and 17 352-cm^{-1} peaks progressions is not included in the average. The $\hbar\omega(t_{1u}^{400}) + n\hbar\omega(a_{1g}^{410})$ peaks with $n > 4$ are too weak to be resolved (see Figure 3c). They are not included in the average.

Results

1. Emission Spectra. The emission spectrum of $[Ph_4P][Ta(CO)_6]$ at 15 K, shown in Figure 1, shows well-resolved vibronic structure in a low-frequency progression starting at 19 130 cm^{-1} with spacings of 410 $\pm$ 10 cm^{-1} (see Table 1). A gap of 540 cm^{-1} is observed adjacent to and lower in energy than the 17 892-cm^{-1} peak. A second set of vibronic progressions with a separation between peaks of 410 $\pm$ 10 cm^{-1} is observed on the low-energy side of the spectrum. The peak maxima and vibrational spacings are listed in Table 1.

The emission spectrum is independent of the excitation wavelength. Irradiation of the sample with the 363.8-, 457.9-, 488.0-, 496.5-, and 514.5-nm output from an argon ion laser produced spectra identical to that in Figure 1.

Changing the sample temperature from 15 to 100 K results in broadening of the vibronic peaks and a loss of resolution,

(10) Dewey, C. G.; Ellis J. E.; Fjare, K. L.; Pfahl, K. M.; Warnock, G. F. P. *Organometallics* **1983**, *2*, 388.
(11) Calderazzo, F.; Englert, U.; Pampaloni, G.; Pelizzi, G. Zamboni, R. *Inorg. Chem.* **1983**, *22*, 1865.

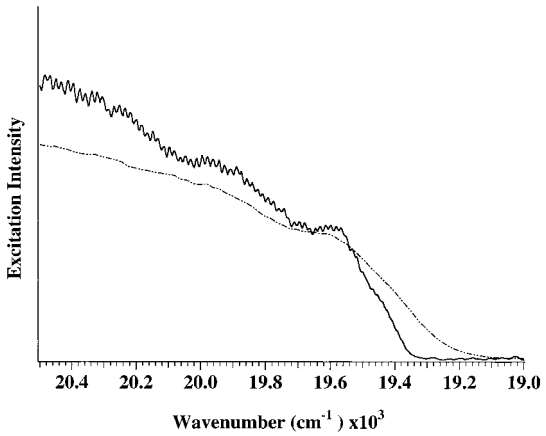

Figure 2. Excitation spectrum of $[Ta(CO)_6]^-$ taken at 77 (dashed line) and 15 K (solid line).

but the band envelope remains constant. Both the red and blue progressions have the same temperature dependence and the loss in resolution and intensity tracked identically for both sets of peaks.

Luminescence spectra of the sample in frozen methyltetrahydrofuran glass are almost identical to those from the solid. The resolution of the vibronic bands did not improve, and the relative intensities remained the same.

2. Excitation Spectra. The excitation spectrum of $[Ph_4P][Ta(CO)_6]$ taken at 15 K that is obtained using a tunable pulsed OPO as the pump source is shown in Figure 2. The spectrum contains a shoulder at approximately 19 450 cm^{-1} and a peak at 19 610 cm^{-1}. At higher energy there is a broad peak centered at 19 980 cm^{-1} with a small shoulder at approximately 19 880 cm^{-1}. No other resolved vibronic structure is observed in the spectrum.

Identical spectra are obtained when the emission is monitored in both the "blue" and "red" regions of the emission spectrum. The peaks that are monitored are at 18 325 (the third vibronic peak in the blue progression), 14 000 (the low-energy wing in the red progression), and 16 878 cm^{-1} (the second vibronic peak in the red progression). All of these excitation spectra contain the same features.

The 77 K continuous-wave excitation spectrum monitored at 18 325 cm^{-1} has features similar to but broader than those in the pulsed spectrum, as shown in Figure 2. Poorly resolved vibronic structure similar to the pulsed laser excitation is observed. The spectrum has an obvious shoulder at 19 610 cm^{-1} and other poorly resolved features at 19 880 and 19 980 cm^{-1}. A very weak and broad shoulder is found at approximately 19 450 cm^{-1}. This shoulder is not as pronounced in the 77 K spectrum as in the 15 K spectrum, but it is clearly distinguishable.

3. Emission Lifetime. Measurements of the 15 K luminescence lifetimes at 18 768 cm^{-1}, the second vibronic peak in the first progression, and 16 515 cm^{-1}, the fourth vibronic peak in the second progression, give values of 15 ± 3 μs. The luminescence follows a single-exponential decay rate.

4. Vibrational Spectra. The vibrational frequencies obtained from Raman spectra of the room-temperature solid excited at 676.4 nm are listed in Table 2. Frequencies and assignments from infrared spectroscopy and theoretically calculated frequencies are also listed.

The 415-cm^{-1} vibration in the Raman spectrum is assigned as the symmetric metal−ligand stretching mode. The 1885-cm^{-1} vibration in the Raman spectrum is assigned to the totally symmetric carbonyl stretching mode. Assignments of the infrared-active vibrational modes have been published.[7] The 410- and 1845-cm^{-1} vibrations are assigned to the asymmetric metal−ligand and carbonyl stretching modes, respectively. On the basis of the calculated normal-mode frequencies, a low-frequency C−M−C bending mode is expected to occur at 80 ± 10 cm^{-1}.[12]

Table 2. Vibrational Frequencies (cm^{-1}) for $[Ta(CO)_6]^-$

Raman

$[Ta(CO)_6]^-$				
obsd[a]	calcd[c]	$W(CO)_6$ [d]	assignment [d]	symmetry [d]
82	70	107	δ (C−Ta−C)	t_{2g}
405	390	418	ν_{as} (Ta−C)	e_g
415	398	433	ν_s (Ta−C)	a_{1g}
1875	1883	1998	ν_{as} (CO)	e_g
1885	1995	2115	ν_s (CO)	a_{1g}

Infrared

$[Ta(CO)_6]^-$				
obsd [b]	calcd [c]	$W(CO)_6$[d]	assignment [d]	symmetry[d]
	62	91	δ (C−Ta−C)	t_{1u}
410	377	374	ν_{as} (Ta−C)	t_{1u}
	496		δ (Ta−CO)	t_{2u}
555	552	586	δ (Ta−CO)	t_{1u}
1845	1868	1997	ν_{as} (CO)	t_{1u}

[a] This work. [b] Reference 7. [c] Reference 12. [d] Jones, L. H.; McDowell, R. S.; Goldblatt, M. *Inorg. Chem.* **1969**, *8*, 2349.

Discussion

1. General Features of the Emission Spectrum. The emission spectrum of $[Ph_4P][Ta(CO)_6]$ in Figure 1 superficially appears to be a simple example of a spectrum containing a vibronic progression in a low-frequency mode. The frequencies of the vibronic bands almost support that view (Table 1); the peaks have an average separation of 410 ± 10 cm^{-1}, consistent within the experimental uncertainty with the 415-cm^{-1} A_{1g} mode observed in the Raman spectrum. However, more careful scrutiny of the spectrum and the table reveals that there is an unexpectedly large gap between the peaks at 17 892 and 17 352 cm^{-1}. A single progression in a 410-cm^{-1} mode cannot fit the spectrum. A simple possible explanation for the gap is that there are two progressions. The first progression produces the "blue" peaks. The second progression begins with one quantum of the 1885-cm^{-1} CO stretching vibration and accounts for the gap. However, this explanation cannot account for the observed intensities in the second set of peaks as shown in Figure 3a.

A second possible vibronic model that better explains the gap and the intensities is that the red set of peaks begins with one quantum of a 1445-cm^{-1} normal mode as shown in Figure 3b. Although this model produces a much better fit, there is no 1445-cm^{-1} vibrational mode in the molecule.

The correct explanation of the vibronic structure is that both sets of progressions are based on different false origins. The details are discussed in section 3. The octahedral molecular symmetry of $[Ta(CO)_6]^-$ requires the presence of asymmetric promoting modes in order to induce the dipole-forbidden ligand field electronic transition. Electronic transitions between Laporte forbidden electronic states, which are dipole forbidden, can become vibronically allowed by asymmetric promoting modes. The electronic origin of the spectrum is located 400 cm^{-1} to higher energy of the first vibronic band. The blue progression is based on a false origin from a 400-cm^{-1} promoting mode,

(12) Jonas, V.; Thiel, W. *Organometallics* **1998**, *17*, 353.

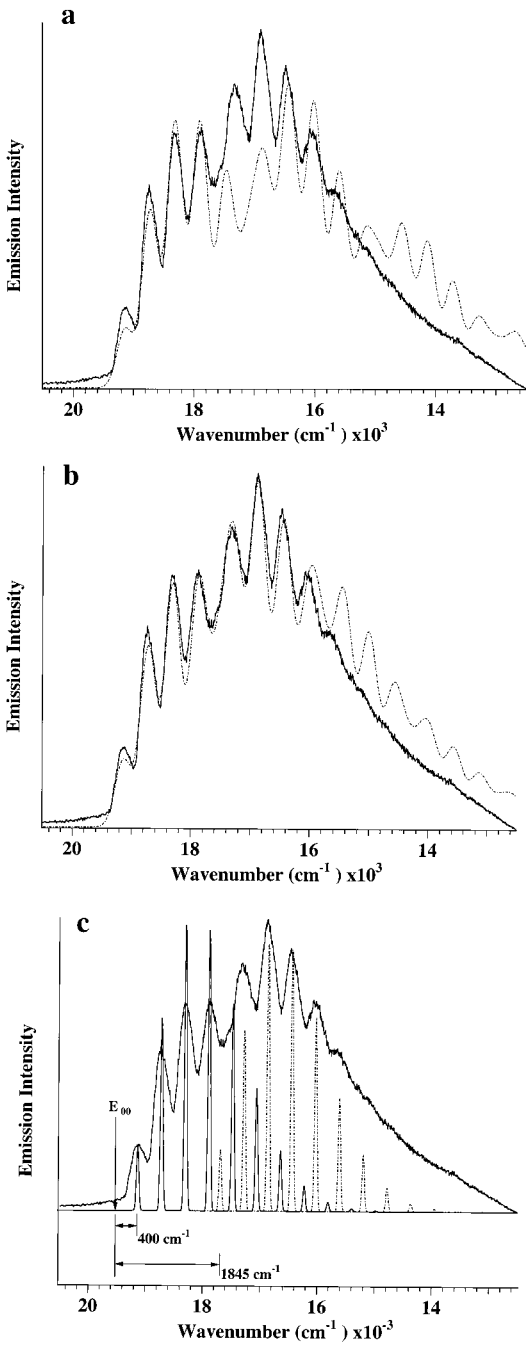

Figure 3. Comparisons of the experimental emission spectrum with calculated spectra based on simple models. (a) The calculated spectrum has its origin at 19 130 cm^{-1} and contains progressions in 410- and 1885-cm^{-1} modes. (b) The calculated spectrum has its origin at 19 130 cm^{-1} and contains progressions in 410- and 1445-cm^{-1} modes. (c) The calculated spectrum has its origin at 19 530 cm^{-1}. An asymmetric 400-cm^{-1} promoting mode produces a false origin at 19 130 cm^{-1} for a progression in a 410-cm^{-1} mode. A second asymmetric promoting mode with a frequency of 1845 cm^{-1} produces a false origin at 17 685 cm^{-1} for the 410-cm^{-1} progression. The best fit using this model is shown in Figure 8.

and the red progression is based on a 1845-cm^{-1} promoting mode. A diagram illustrating these features is shown in Figure 3c.

An alternative explanation is the presence of two independently emitting states or species. For example, two different spin−orbit states could contribute to the spectrum, or two different crystal sites could be involved. The energy separation between the blue and red sets of peaks is large, and it is unlikely that crystallographic sites or spin−orbit coupling could cause an energy separation of this magnitude. These possibilities must be eliminated before more complicated vibronic coupling mechanisms can be proposed and examined.

2. Absence of Multiple States or Sites. Possible explanations for the red and blue luminescence bands are emission from two electronic states, emission from two different molecules (impurities), or emission from molecules in different sites in the crystal. The photophysical experiments discussed below are used to eliminate these explanations.

Excitation Spectra. The existence of multiple luminophores can frequently be determined by analyzing the excitation spectra. The excitation spectrum obtained by monitoring the blue emission should be different from that obtained by monitoring the red emission. Energy transfer could complicate the interpretation, but the excitation spectrum obtained by monitoring the red emission should be unambiguous. If the red emission arises from a molecule or excited state different from that responsible for the blue emission, then excitation intensity should be observed in the region of its spectral origin (i.e., lower in energy than the spectral origin of the blue band). Excitation spectra taken when monitoring at 16 878 and 14 000 cm^{-1} in the red emission band, and at 18 325 cm^{-1} in the blue emission band, are identical. No excitation intensity was observed in the region where the spectral origin of the red emission should be.

Excitation spectra were also obtained with a CW source at 77 K. Identical spectra were obtained by monitoring the red and the blue regions. The existence of identical spectra when both the blue and red progressions are monitored strongly argues against emission from two molecules, two sites, or two states. Different molecules would have different electronic origins, and hence the individual luminescence spectra could be selectively irradiated.

Luminescence Lifetimes. Two different electronic states, molecules, or sites may have different luminescence lifetimes. However, the lifetimes measured when monitoring the red or the blue emissions are 15 ± 3 μs, identical within the experimental uncertainty. The fact that both the blue and red regions have the same excited-state lifetime supports a one-electronic-state model. The lifetime measurements do not conclusively prove the absence of two emitting states or molecules because they could fortuitously have the same lifetimes, but they are consistent with the one-state explanation.

Temperature Dependence of the Luminescence Spectrum. Temperature-dependent emission spectra could reveal the existence of two emitting states or molecules if the effects on the spectra were different for the two entities. For example, radiationless deactivation processes could be quite different and could result in changes in the relative intensities of the red and blue bands as a function of temperature. However, the experimental spectra taken at temperatures ranging from 15 to 100 K showed that the intensities of both sets of progressions decrease identically as the temperature is raised. In addition, the emission band maxima do not change. The major effects of increasing the temperature are to decrease the resolution by broadening the vibronic peaks and to decrease the emission intensity. The fact that varying the temperature causes both the red and blue progressions to change identically supports the one-state explanation of the emission.

Luminescence Spectra in Frozen Organic Glass. If the origins of the red and blue emissions were two different crystal sites, then spectra obtained in frozen organic glasses should contain only one set of progressions. By dissolving the sample in methyl-THF and freezing at 15 K to form a glass, individual

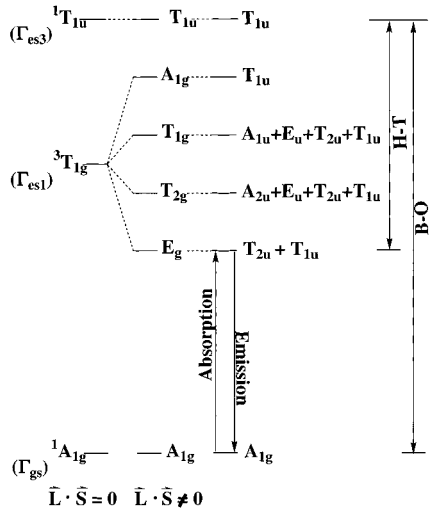

Figure 4. State diagram for $[Ta(CO)_6]^-$. The lowest ligand field excited state ($^3T_{1g}$) and a metal-to-ligand charge-transfer state ($^1T_{1u}$) are illustrated in the absence of spin−orbit coupling (left side), including spin−orbit coupling (middle), and including vibronic coupling with the asymmetric t_{1u} normal mode (right side). The double-headed arrows indicate the states involved in Herzberg−Teller (H−T) and Born−Oppenheimer (B−O) coupling.

molecules are isolated and possible effects from crystal defect sites are removed. No changes in the relative intensities of the red and blue regions were observed in the glass spectra. These observations prove that crystal sites are not the cause of the red and blue emissions.

Solid-State Raman Spectra. Solid-state Raman spectra further support the absence of markedly different crystal sites. If there were a large population of such sites, Raman bands (particularly the CO stretching bands) would show broadening, shifting, or splitting. The experimental spectra contain only sharp peaks with no splitting or satellites.

In summary, the experimental observations of identical excitation spectra, a single luminescence lifetime, no relative intensity changes as a function of temperature, and no change in the relative intensities in the frozen glass are all consistent with a single emitting state from the $[Ta(CO)_6]^-$ ion.

3. Selection Rules and Vibronic Interactions. The excited electronic states that are involved in the emission and excitation spectra and in vibronic coupling of the $[Ta(CO)_6]^-$ ion are shown in Figure 4. In O_h symmetry, the ground-state electron configuration is $(t_{2g})^6$, giving rise to a $^1A_{1g}$ ground state. The lowest energy excited electron configuration is $(t_{2g})^5(e_g)^1$, giving rise to both singlet and triplet T_{1g} and T_{2g} excited states. The $^3T_{1g}$ state is the lowest energy excited electronic state.[13,14] The absorption band with a maximum at 22 220 cm^{-1} has been assigned to the $^1A_{1g} \rightarrow {}^3T_{1g}$ transition,[7] and the next highest band at 24 200 cm^{-1} to the $^1A_{1g} \rightarrow {}^1T_{1g}$ transition.[7,13] A strong absorption at 26 180 cm^{-1} was assigned to the metal−ligand charge-transfer $^1A_{1g} \rightarrow {}^1T_{1u}$ transition.[7,15] The lowest energy transition in $[Ta(CO)_6]^-$ is both spin and Laporte forbidden. Spin−orbit coupling is large in third-row transition metal complexes ($\zeta = 1657$ cm^{-1} for Ta(0)), and the singlet and triplet spin multiplicity designations lose their meaning. The spin−orbit states that arise from the $^3T_{1g}$ state are shown in the middle of Figure 4. The order that is shown, with $E_g(\Gamma_3)$ as the lowest energy spin−orbit excited state, is chosen by analogy with calculated orders for other octahedral d^6 metal complexes.[14] The electric dipole operator $e\hat{r}$ transforms as t_{1u} in the O_h point group, and thus the $g \rightarrow g$ transitions to the spin−orbit states are forbidden. The transitions become allowed via vibronic coupling involving an ungerade vibrational mode. The ungerade normal modes in octahedral molecules are t_{1u} and t_{2u}; the irreducible representations of the vibronic states involving the t_{1u} mode are shown next to the respective spin−orbit states. The $A_{1g} \rightarrow T_{1u}$ ($E_g \times t_{1u}$ from the $^3T_{1g}$ electronic state) is now electric dipole allowed.

The group theoretical calculation specifies which normal modes can make the transition allowed, but it does not offer any insight into the details of the mechanism. Common mechanisms for inducing nonzero transition dipoles are Herzberg−Teller (H−T) coupling and Born−Oppenheimer (B−O) coupling.[16,17] According to this treatment, the asymmetric motion causes mixing between the formally forbidden state (the E_g spin−orbit-coupled ligand field state in our case) and an allowed state. In the example under consideration here, the fully allowed state is the $^1T_{1u}$ metal−ligand charge-transfer state.

Two forms of the mixing have been discussed.[16] The classic H−T coupling involves mixing of the forbidden excited state with a nearby allowed excited state. This mixing is shown by the double-headed arrow labeled HT in Figure 3 that connects the forbidden E_g excited state with the allowed T_{1u} excited state. B−O coupling, on the other hand, involves mixing of the ground state with the allowed excited state.[16] This mixing is illustrated with the double-headed arrow labeled B−O connecting the A_{1g} ground state with the allowed T_{1u} excited state. The energy separation between these states is much larger than that between the two excited states. In both the H−T and B−O mechanisms, vibronic coupling with the t_{1u} vibration is needed to mix the two states of different parity.[18] Because the energy separation between the two states that mix is smaller in H−T coupling, this coupling is often assumed to dominate. However, arguments have been presented that suggest that B−O coupling can have an equal or greater magnitude.[16]

The simplest treatment of vibronic coupling assumes that the molecular Hamiltonian is separable into electronic and nuclear Hamiltonians H_e and H_n, and that H_e varies slowly with changes in the nuclear coordinates. The effect of the dependence on nuclear coordinates is expressed as a Taylor series expansion, where Q_i is the ith normal coordinate. The H−T transition dipole

$$H_e = (H_e)_o + \sum_i \left(\frac{dH_e}{dQ_i}\right)_o Q_i + \cdots \qquad (1)$$

μ for a transition from ground state Ψ_{gs} to an excited state Ψ_{es} through mixing with a third state Ψ_i is given by[16]

$$\mu = \sum_i \frac{\langle \Psi_{gs}|er|\Psi_i\rangle \langle \Psi_i|(dH_e/dQ_i)_o|\Psi_{es}\rangle}{[E_i - E_n]} \qquad (2)$$

Because H_e is totally symmetric, $(dH_e/dQ_i)_o$ transforms as Q_i and can mix ungerade functions into gerade functions. From the analysis in Figure 4, one quantum of vibration in a t_{1u} mode will make the transition between the A_{1g} ground state Ψ_{gs} and the E_g excited state Ψ_{es} allowed with vibronic mixing with the T_{1u} excited state Ψ_i.

(13) Beach, N. A.; Gray, H. B. *J. Am. Chem. Soc.* **1968**, *90*, 5713.
(14) Hakamata, K.; Urushiyama, A.; Kupka, H. *J. Phys. Chem.* **1981**, *85*, 1983.
(15) Gray, H. B.; Beach, N. A. *J. Am. Chem. Soc.* **1963**, *85*, 2922.
(16) Orlandi, G.; Siebrand. W. *J. Chem. Phys.* **1973**, *58*, 4513.
(17) Gregory, A. R.; Siebrand, W.; Zgierski, M. Z. *J. Chem. Phys.* **1976**, *64*, 3145.
(18) Flint, C. D. *Coord. Chem. Rev.* **1974**, *14*, 47.

Simple symmetry considerations do not offer insight into which of the normal modes of proper symmetry are most important. In the case of the $[Ta(CO)_6]^-$ ion, the electronic states that mix involve one that is primarily metal centered and the other that has a large ligand contribution. Thus, it might be expected that both metal−ligand and CO vibrations with t_{1u} symmetry could be involved. The experimental results discussed below show that a metal−ligand torsional mode, a metal−ligand stretching mode, and a CO stretching mode are all involved.[16,18−19]

4. Time-Dependent Theoretical Treatment of Vibronic Coupling. A. Calculation of Absorption and Emission Spectra. Spectra are calculated by using the split operator technique of Feit and Fleck[20−22] and the time-dependent theory of electronic spectroscopy. The derivation of the time-dependent theory has been published, so only a brief review of the equations used in this paper will be given.[23−25] The spectra are governed by the motion of a wave packet on a multidimensional potential energy surface. When a photon is emitted or absorbed, a wave packet ϕ is created at time $t = 0$ on the final potential energy surface. The final potential energy surface is, in general, displaced relative to the initial potential energy surface along normal vibrational coordinates and has a form (force constant) different from that of the initial surface. The wave packet is not generally an eigenfunction of the final surface and develops in time according to the time-dependent Schrödinger equation. The intensity of an electronic transition is given by eq 3,

$$I(\omega) = C\omega^n \int_{-\infty}^{+\infty} \exp(i\omega t)\left\{\langle\phi|\phi(t)\rangle \exp\left(-\Gamma^2 t^2 + \frac{iE_{00}}{\hbar}t\right\}\right. \mathrm{d}t \tag{3}$$

where $I(\omega)$ is the emission intensity in photons per unit volume per unit area at frequency ω, and C is a proportionality constant. E_{00} is the energy of the electronic origin transition, and Γ is a phenomenological Gaussian damping factor. The calculation of the intensity is similar for both absorption and emission transitions, except for the dependency on the emitted radiation frequency. The intensity in an electronic absorption transition is proportional to ω, while an emission transition has a cubic dependency on the frequency.

The most important quantity of interest in eq 3 is the time-dependent overlap $\langle\phi|\phi(t)\rangle$, where $|\phi\rangle = \mu|\chi\rangle$ is the lowest energy vibrational eigenfunction of the initial state $|\chi\rangle$ multiplied by the transition dipole moment μ, and $|\phi(t)\rangle = \exp(-iH_{ext}t/h)|\phi\rangle$ is a moving wave packet propagated by the final state Hamiltonian. In the case of HT coupling, the dipole moment is not a constant as in the case of an allowed transition, but rather it is a function of the normal coordinate $\mu = \mu(Q)$. The functional form of the dipole moment is discussed in the next section.

The overlap function $\langle\phi|\phi(t)\rangle$ is calculated by numerical integration of the time-dependent Schrödinger equation according to the method of Feit and Fleck.[21] The overlap is calculated by a two-dimensional set of grid points. The grid consists of increments in the normal coordinate ΔQ in one dimension and time increments of Δt in the other dimension. The equations describing how the overlap function is calculated after each Δt is shown in eq 4:

$$\phi(t + \Delta t) = \exp\left(\left(\frac{i\delta t}{4M}\right)\nabla^2\right) \exp(-i\delta t V) \exp\left(\left(\frac{i\delta t}{4M}\right)\nabla^2\right)\phi(Q,t) + O[(\Delta t)^3] \tag{4}$$

The value of the overlap is calculated for each normal coordinate, and the overlap functions are multiplied to give the final overlap function as illustrated in eq 5:

$$\langle\phi|\phi(t)\rangle = \prod_k \langle\phi_k|\phi_k(t)\rangle \tag{5}$$

The final $\langle\phi|\phi(t)\rangle$ is then Fourier transformed according to eq 3.

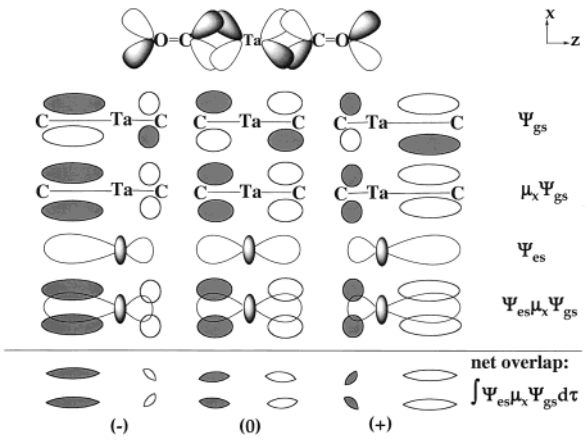

Figure 5. Illustration of the transition dipole moment in the *z* direction as a function of the asymmetric t_{1u} normal coordinate with *x*-polarized light. The top line shows the orbital overlap of the metal d_{xz} orbital with the CO π^* orbital in the ground electronic state. The second line is a simplified sketch of the ground-state probability contour. The third line shows the ground-state orbitals multiplied by the transition dipole moment in the *x* direction. The fourth line shows the representation of the ligand field excited state by the d_{z^2} probability contour. The fifth line shows the product of the ground electronic state, the dipole, and the ligand field excited state. The sixth line is the net overlap and is the pictorial representation of the transition dipole moment.

B. Coordinate Dependence of μ and Vibronic Coupling. The transition dipole moment is given by $\mu = \int\Psi_{es}e\hat{r}\Psi_{gs}$ for electronic transitions between the ground and excited states. The physical meaning of μ can be explained in a simple way by using qualitative electron density diagrams to represent the excited and ground electronic states Ψ_{es} and Ψ_{gs} as shown in Figure 5. The electronic dipole moment operator $e\hat{r}$ is represented by a function that changes sign at the origin. This type of pictoral representation was used to illustrate the symmetries of the transition dipole moment for the water molecule[26] and for intervalence electron-transfer transitions.[27]

The pictorial representation of the transition dipole moment for the ligand field transition along the t_{1u} coordinate is shown in Figure 5. The electron density of the ground electronic state along the *z* axis is shown at the top of the figure. (The other axes are identical.) The probability contours represent the π back-bonding interaction between the d_{xz} orbital and the unoccupied orbital of π symmetry on the carbonyl ligands. A negative sign of the wave function is represented by the shaded area.

To represent μ for *x*-polarized light (the direction in the plane of the paper perpendicular to the line of atoms shown), the *x*

(19) Albrecht, A. C. *J. Chem. Phys.* **1979**, *70*, 2644.
(20) Kosloff, D.; Kosloff, R. *J. Comput. Phys.* **1983**, *52*, 35.
(21) Feit, M. D.; Fleck, J. A.; Steiger, A. *J. Comput. Phys.* **1982**, *47*, 412
(22) Tannor, J. *J. Chem. Educ.* **1990**, *67*, 917.
(23) Heller, E. J. *J. Chem. Phys.* **1978**, *68*, 2066.
(24) Heller, E. J. *J. Chem. Phys.* **1978**, *68*, 3891.
(25) Heller, E. J. *Acc. Chem. Res.* **1981**, *14*, 368.
(26) Tannor, D. J. *J. Phys. Chem.* **1988**, *92*, 3341.
(27) Talaga, D. S.; Zink, J. I. *J. Phys. Chem.* **1996**, *100*, 12.

component of the electric dipole operator causes a sign change in the *x* direction. Thus, $\mu_x\Psi_{gs}$ is represented as contours with a change of sign below the *yz* plane.

The excited electronic state, shown in the third row, is represented by the d_{z^2} orbital. It undergoes out-of-phase overlap with the σ donor orbital of the carbonyl ligands. This orbital is metal−ligand antibonding. The product $\Psi_{es}\mu\Psi_{gs}$ is shown in the fourth row, and the overlap $\int\Psi_{es}\mu\Psi_{gs}\,dr$ is shown in the bottom row. The overlap is the pictorial representation of the transition dipole.

The most important feature of the overlap is that its value is zero at $Q = 0$. (There are equal amounts of positive and negative overlap.) The physical meaning is that the transition is electric dipole forbidden at the equilibrium internuclear geometry.

The left and right sides of the figure illustrate the effect of vibration along the t_{1u} coordinate. The motion of one of the partners of the triply degenerate vibration is shown; the other partners have equivalent motions along the other two axes. To represent an elongated metal−ligand bond as the right side of the molecule elongates, the contours are elongated. Bond contraction results in analogous contraction of the contours. The extremes of the displacements are shown on the left and right sides of the figure.

The effects of the motion on the overlap are shown in the fifth line of the figure. At Q = 0, there are equal amounts of positive and negative overlap, resulting in a net overlap of zero. On the right side of the figure, the positive overlap resulting from elongation of the metal−ligand bond on the right side of the molecule is greater than the negative overlap on the left side of the molecule. The net result is positive overlap and thus a positive nonzero transition dipole. The opposite effect is shown on the left side of the figure; the net result is negative overlap and a negative nonzero transition dipole. The interpretation of this behavior of μ is that the transition is electric dipole forbidden at $Q = 0$ but vibronically allowed.

The analysis of the transition dipole moment along the totally symmetric normal coordinate is similar. In this case, both sides of the molecule elongate or contract equally. The positive and negative overlaps also change equally, and the total remains zero. Thus, the transition dipole moment is always zero, and the transition is dipole forbidden.

C. Calculation of Vibronically Allowed Transitions Using Time-Dependent Theory. The wave packet that is propagated, $\mu|\chi\rangle$, in the calculation of the electronic emission spectrum is zero at the origin and changes sign at the origin in the case of the t_{1u} coordinate in O_h symmetry. A sketch of the initial vibrational wave function and the wave packet $\mu|\chi\rangle(t = 0)$ is shown in Figure 6. The exact numerical form of μ is not known in general and must be calculated or determined experimentally on a case-by-case basis. Several different functional forms have been suggested.[26−28] In this paper, the simplest form, a linear function of the coordinate, is chosen. This choice does not result in any loss of generality in the following calculations because the emission quantum yield is not being calculated. A coordinate-dependent transition dipole is easily incorporated in the time-dependent calculations, and this simplicity is a powerful advantage of these types of calculations. Most of the calculations of spectra to date have involved allowed transitions where the Condon approximation (a constant transition dipole) is a good approximation and the value of μ is part of the constant in eq 3.

The cross section of the initial and final potential surfaces along the t_{1u} asymmetric coordinate is shown in Figure 6. The minima of the ground- and excited-state surfaces are undisplaced as required by symmetry, but the force constants are different. The wave packet is not an eigenfunction of the excited surface; the absolute value of the time-dependent overlap is shown in the middle panel. Note that there is a recurrence after one vibrational period as usual, but that in addition there is a recurrence at half of the vibrational period. A simple physical picture suggests that the positive and negative wings interchange position after half a vibrational period, resulting in a negative (out-of-phase) overlap, and then return to their original positions, resulting in a positive overlap. After Fourier transformation to give the spectrum (bottom panel), the first recurrence results in a separation of peaks in the frequency domain of twice the vibrational frequency, and the phase results in an offset by one vibrational frequency. The requirement of group theory that only the odd quanta will have nonzero intensity is met.

The relative intensities of the peaks in a given spectrum are dependent on the functional form and the difference between the force constants of the potential surfaces. For typical force

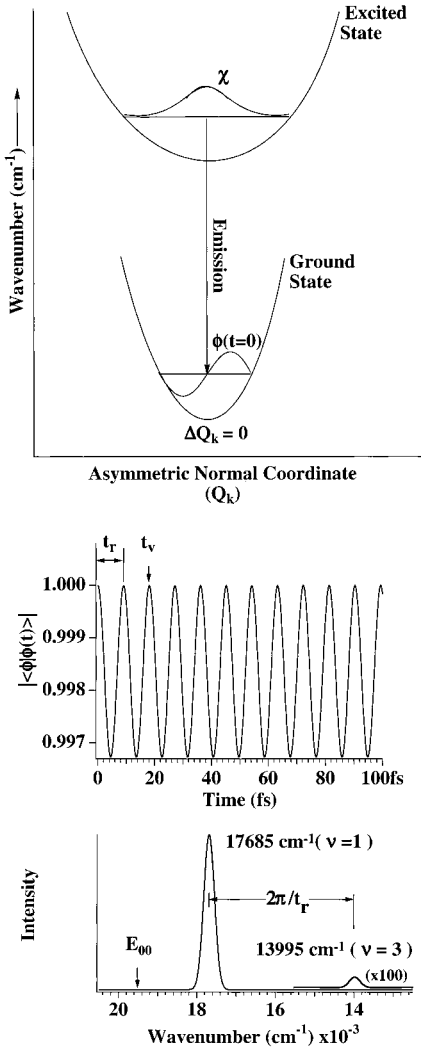

Figure 6. Ground- and excited-state potential energy surfaces along asymmetric normal coordinates. The top panel illustrates the wave packet on an undisplaced potential energy surface. The middle panel is the magnitude of the overlap with no damping. The first recurrence is labeled t_r, and one vibrational period is labeled t_v. The bottom panel is the Fourier transform of the overlap function showing the energy of the vibronic origin and the peaks from odd-quanta vibrational states. A damping function that makes the overlap reach 1/*e* of its initial value in 55.4 fs is included in the Fourier transform.

(28) Zhang, J. Z.; Heller, E. J.; Huber, D.; Imre, D. G. *J. Phys. Chem.* **1991**, *95*, 6129.

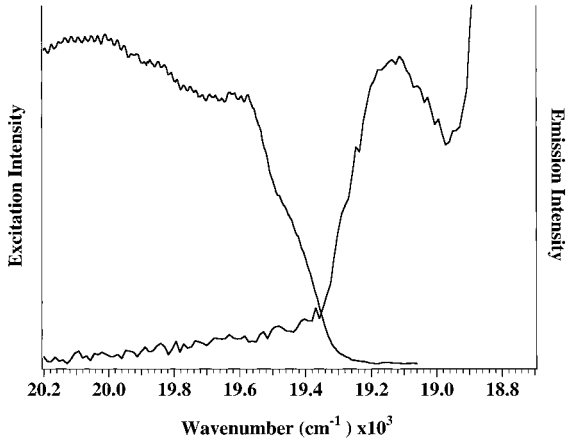

Figure 7. Excitation (left) and emission (right) spectra taken at 15 K showing the vibronic peaks nearest the electronic origin.

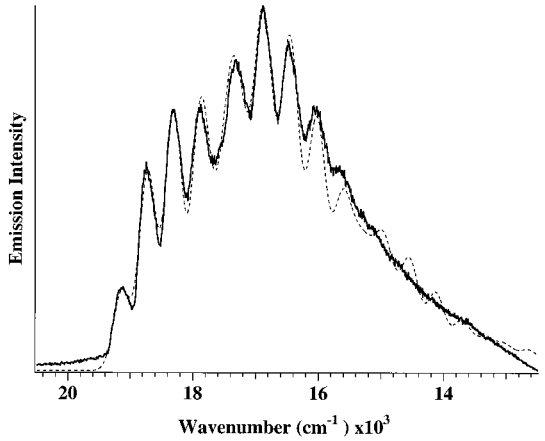

Figure 8. Experimental emission spectrum (solid line) and calculated best-fit emission spectrum (dashed line).

constant changes (on the order of 10%) and a linear coordinate dependence of μ, the first peak is on the order of 100−1000 times more intense than the other peaks.

The complete spectrum for a molecule with multiple displaced symmetric modes and an undisplaced asymmetric mode is calculated by Fourier transforming the product of the overlaps for all of the modes (eq 3.) The result will be a spectrum with no intensity at E_{00} and a "false origin" at E_{00} + one quantum of the asymmetric mode frequency, followed by the usual progressions in the symmetric modes. The next false origin, at E_{00} + three quanta of the asymmetric mode's frequency, will be at least a factor of 100 smaller.

5. Quantitative Calculations of the Emission Spectrum and Excited-State Distortions of $[Ta(CO)_6]^-$. A. False Origins and Location of the Electronic Origin. The emission spectrum contains two false origins. The first is at 19 130 cm^{-1} (the origin of the "blue" progression in Figure 1), and the second is at 17 685 cm^{-1} (the "red" progression"). These vibronic origins are consistent with the known frequencies of the t_{1u} modes if the electronic origin of the spectrum, E_{00}, is at 19 530 cm^{-1}. The blue progression begins with one quantum of the 400-cm^{-1} t_{1u} mode and 0, 1, 2, ... quanta of the totally symmetric 410-cm^{-1} mode. The red progression begins with one quantum of the 1845-cm^{-1} t_{1u} mode and 0, 1, 2, ... quanta of the totally symmetric 410-cm^{-1} mode. These H−T active t_{1u} modes involve normal modes of the final electronic state (in this case the ground state). The low-frequency t_{1u} torsional mode does not play a major role in the emission spectrum.

The first prominent peak in the excitation spectrum is found at 19 610 cm^{-1} as shown in Figure 7. The energy separation between this peak and the first peak in the emission spectrum is 480 cm^{-1}. For vibronically allowed spectra, this energy separation is most commonly the sum of the frequencies of one promoting mode in ground and excited states. The observed 480-cm^{-1} separation is much too small to be the sum of the excited- and ground-state asymmetric metal−ligand-promoting mode frequencies. However, for H−T coupling, the normal mode that causes the largest coupling between the final state and the allowed state for emission is not necessarily the same as that which couples the final and allowed states in absorption (or excitation). In the case of $[Ta(CO)_6]^-$, the low-frequency t_{1u} torsional mode is obviously important in the excitation spectrum. The 480-cm^{-1} energy separation is the sum of the 80-cm^{-1} t_{1u} mode that promotes the excitation and the 400-cm^{-1} mode that promotes the emission. The first major peak in the excitation at 19 610 cm^{-1} is thus one quantum of the 80-cm^{-1} t_{1u} mode and zero quanta of the symmetric M−C stretching mode. A progression in a 370-cm^{-1} totally symmetric mode is observed in the excitation spectrum corresponding to 0, 1, 2, ... quanta of this symmetric stretch. The Ta−C totally symmetric stretching frequency in the excited electronic state is reduced from that in the ground state by 40 cm^{-1}.

A weak shoulder is found in the excitation spectrum at 19 450 cm^{-1}, and weak emission intensity at that wavenumber is observed in the emission spectrum. This shoulder in the excitation spectrum is attributed to thermal population of the low-frequency t_{1u} mode (a hot band). Thermal population of this mode in the excited state and/or weak H−T activity may cause the low-intensity emission in this region.

The t_{1u} M−C stretching mode is probably also active in the excitation spectrum. The shoulder at 19 880 cm^{-1} is probably a result of one quantum of this mode; its frequency is 350 cm^{-1}, reduced by 50 cm^{-1} in the excited electronic state. It is difficult to assign the peaks with certainty because two H−T modes and one thermally populated mode cause the excitation spectrum to become congested even in the region near the origin.

B. Fitting of the Emission Spectrum. The fit of the emission spectrum uses two asymmetric t_{1u} modes, two totally symmetric modes, and the electronic origin E_{00} located at 19 530 cm^{-1}. The overlap function for each asymmetric mode is calculated by using an undisplaced excited-state potential energy surface and a transition dipole moment with a linear coordinate dependence. The time-dependent overlap functions for displaced totally symmetric 410-cm^{-1} metal−ligand and 1885-cm^{-1} carbonyl stretching modes are calculated using a constant transition dipole moment along the symmetric coordinates. The overlap functions for each normal mode are multiplied according to eq 5, and the total overlap function is Fourier transformed as in eq 3.

The best fit of the emission spectrum uses the following parameters. The asymmetric vibrational modes were calculated using a dimensionless distortion $\Delta = 0$ as required by symmetry. The totally symmetric normal modes were calculated using dimensionless distortions of $\Delta = 2.52$ for the 410-cm^{-1} Ta−C stretch and $\Delta = 1.05$ for the 1885-cm^{-1} CO stretch. The value of the damping factor that best fits the vibronic bandwidth is $\Gamma = 96$ cm^{-1}. The calculated emission spectrum is superimposed on the experimental spectrum in Figure 8. An excellent fit is obtained.

C. Excited-State Distortions. The dimensionless distortions Δ obtained from the calculation of the emission spectrum can be converted to bond length changes in angstrom units when the normal coordinates and the potential energy distributions are known. The bond length changes can be estimated if some

simplifying assumptions are made. For example, if it is assumed that the 410-cm^{-1} normal mode is entirely M−CO stretching and that the normal mass is the mass of the CO ligand, then the dimensionless distortions, Δ, can be converted into distortions in angstroms, $\Delta\delta$, by using the equation

$$\Delta\delta_i = \left(6.023 \times 10^{23}\frac{\hbar}{2\pi c\omega m}\right)^{1/2}(10^8\Delta_i) \qquad (6)$$

where m is the mass involved in the vibration in units of gram atomic weight (e.g., CO = 28 g), ω is the wavenumber of the vibrational mode in cm^{-1}, $\hbar = h/2\pi$, where h is Planck's constant in g cm^2 s^{-1}, c is the speed of light in cm s^{-1}, $\Delta\delta$ is the displacement in Å, and Δ is the dimensionless distortion. When the dimensionless distortions for $[Ta(CO)_6]^-$ are converted into angstroms, the excited-state bond length changes are 0.14 Å for the Ta−C bond and 0.026 Å for the C−O bond.

Very little is known about bond length changes in excited states of octahedral metal carbonyl complexes. Vibronic progressions were observed in the electronic absorption spectra of $Mo(CO)_6$ and $W(CO)_6$.[29] The excited-state distortions in tungsten hexacarbonyl were 0.15 and 0.04 Å for the W−C and C−O bonds, respectively. The vibrational frequencies decreased by 10 cm^{-1} for the symmetric W−C mode and 284 cm^{-1} for the symmetric C−O mode. Molybdenum hexacarbonyl showed similar distortions of 0.16 and 0.03 Å, respectively, with decreases of 12 cm^{-1} in the Mo−C vibrational frequency and 174 cm^{-1} in the CO vibrational frequency. These changes in bond lengths and frequencies are similar to those calculated for $[Ta(CO)_6]^-$.

Excited-state distortions have also been calculated for some monosubstituted metal carbonyl and metal monocarbonyl complexes. $W(CO)_5L$ compounds containing nitrogen donor ligands showed similar distortions in the M−C and C−O bonds in the lowest energy excited state. An electronic and resonance Raman spectroscopic study of $W(CO)_5$(pyridine) and $W(CO)_5$(piperidine) found that the W−C bonds trans to the amine change by 0.12 and 0.25 Å, respectively, while the bonds in the cis positions alter by 0.04−0.05 Å.[6] TRIR analysis of the same compounds showed that the C−O bond distances increased by 0.006 Å for the trans CO and 0.024 Å for the cis ligands in the pyridine complex. The piperidine complex had similar bonding changes of 0.005 and 0.026 Å for the trans and cis carbonyls.[30] Analysis of the bonding changes in the ligand field excited state of $[PtCl_3(CO)]^-$ showed similar bond distortions in Pt−C.[31] Upon excitation into the excited electronic state, the metal−carbon distance was found to increase by 0.18 Å.

Increases in the carbonyl vibrational frequencies were found when the HOMO is depopulated in valence shell ultraviolet ionization spectra.[32] Ionized excited states observed in the ultraviolet photoelectron excitation spectra of group VIB metal carbonyl compounds showed that, upon removal of an electron from a bonding orbital, the M−C and C−O vibrational frequencies both decrease. The observed frequency changes are approximately 40 cm^{-1} for the M−C vibration[32] and 175 cm^{-1} for the C−O vibration.[33]

6. Summary. The vibronically allowed emission spectrum of $[Ta(CO)_6]^-$ originates from a single ligand field excited state. The apparent energy gap between the red and the blue regions of the spectrum is a result of Herzberg−Teller coupling of the ligand field state, with an allowed metal-to-ligand charge-transfer excited state. Two t_{1u} normal modes, a Ta−C stretching mode and a C−O stretching mode, dominate the H−T coupling. These two modes produce two false origins in the emission spectrum. The absence of two emitting molecules, sites, or excited states (that also could have caused the spectrum to appear to be separated into two regions) is proven by excitation spectroscopy and by temperature, lifetime, and solvent dependence studies of the emission.

Herzberg−Teller coupling is treated by using a coordinate-dependent transition dipole moment. A graphical representation of the transition probability along the asymmetric normal coordinates is developed to illustrate the coordinate dependence and provide a physical explanation. The transition dipole is zero at the equilibrium internuclear geometry (a dipole-forbidden transition) but becomes nonzero along the t_{1u} normal coordinates (a vibronically allowed transition.)

The spectrum is calculated by using the time-dependent theory of electronic spectroscopy and wave packet propagation based on the method of Feit and Fleck. The H−T coupling is treated by a linear coordinate dependence along the undisplaced asymmetric coordinates and a constant (nonzero) dipole along the displaced symmetric coordinates. The change in the Ta−C bond length is 0.14 Å, and that in the C−O bond length is 0.026 Å in the ligand field excited state relative to that in the ground electronic state.

Acknowledgment. This work was made possible by a grant from the National Science Foundation (CHE98-16552). We thank Dr. Y. Y. Yang and Dr. Gary Hollingsworth for assistance.

JA0010305

(29) Trogler, W. C.; Desjardins, S. R.; Solomon, E. I. *Inorg. Chem.* **1979**, *18*, 2131.
(30) Johnson, F. P. A.; George, M. W.; Morrison, S. L.; Turner, J. J. *J. Chem. Soc., Chem. Commun.* **1995**, 391.
(31) Chang, T. H.; Zink, J. I. *J. Am. Chem. Soc.* **1987**, *109*, 692.
(32) Hubbard, J. L.; Lichtenberger, D. L. *J. Am. Chem. Soc.* **1982**, *104*, 2132.
(33) Cooper, G.; Sze, K. H.; Brion, C. E. *J. Am. Chem. Soc.* **1990**, *112*, 4121.